

An *In Situ* GISAXS Study of Selective Solvent Vapor Annealing in Thin Block Copolymer Films: Symmetry Breaking of In-Plane Sphere Order upon Deswelling

Ilja Gunkel,^{1,2*} Xiaodan Gu,^{1†} Zhiwei Sun,¹ Eric Schaible,²
Alexander Hexemer,² Thomas P. Russell^{1,3}

¹Polymer Science and Engineering Department, University of Massachusetts at Amherst, 120 Governors Drive, Amherst, Massachusetts 01003

²Lawrence Berkeley National Laboratory, Advanced Light Source, 1 Cyclotron Road, Berkeley, California 94720

³Lawrence Berkeley National Laboratory, Materials Science Division, 1 Cyclotron Road, Berkeley, California 94720

Correspondence to: T. P. Russell (E-mail: russell@mail.pse.umass.edu) or I. Gunkel (E-mail: ilja.gunkel@unifr.ch)

Received 1 August 2015; accepted 17 September 2015; published online 15 October 2015

DOI: 10.1002/polb.23933

ABSTRACT: Thin films of asymmetric poly(styrene-*b*-4-vinylpyridine) (PS-*b*-P4VP) block copolymers are studied by means of *in situ* grazing-incidence small-angle X-ray scattering (GISAXS) during solvent vapor annealing in tetrahydrofuran, a solvent selective for the PS majority block of the copolymer. Upon swelling, PS-*b*-P4VP block copolymers form hexagonal arrays of spherical P4VP microdomains in a PS matrix in films 7–9 layers thick. Deswelling the films induces a transition from hexagonal to face-centered orthorhombic (fco) symmetry, which is stable only at ~ 7 layers of spherical microdomains. Dry films show co-existing hexagonal and orthorhombic symmetries when the solvent is removed slowly, whereas instantaneous solvent removal suppresses the fco structure, resulting in films with only hexagonal structure. The in-plane order of microdomains is significantly deteriorated in dry

films independent of the solvent removal rate. Spherical block copolymer microdomains are known to undergo a transition from hexagonal to orthorhombic packing in isothermally annealed thin films when the number of sphere layers is increased from 4 to 5. In this paper, *in situ* GISAXS experiments reveal that a similar transition occurs during solvent vapor annealing in a selective solvent. Interestingly, the transition from hexagonal to orthorhombic packing of spheres occurs as solvent is removed from a thin block copolymer film. © 2015 Wiley Periodicals, Inc. *J. Polym. Sci., Part B: Polym. Phys.* **2016**, *54*, 331–338

KEYWORDS: block copolymer thin films; *in situ* grazing incidence small-angle x-ray scattering (GISAXS); selective solvent vapor annealing

INTRODUCTION In 2007, Kramer and coworkers reported a transition from 2D to 3D packing of spherical microdomains in thin films of thermally annealed block copolymers (BCPs) with changing film thickness.^{1,2} Films having thicknesses of four layers of spheres or less were found to have 2D hexagonal symmetry. As the film thickness increased, the hexagonal symmetry was found to change to an orthorhombic packing of spheres and continuously approach a BCC (110) packing as the number of layers of spheres increased. Kramer and coworkers later showed, using self-consistent field theory, that this symmetry transition results from a

competition between the preferred hexagonal packing of spheres at the film surface with the BCC (110) packing preferred in the bulk.² Film thickness and period changes, along with an in-plane frustration due to the finite size of the substrate, also occur during solvent vapor annealing (SVA) as a result of the swelling of the film. In this study we examine the symmetry-breaking in the packing of spherical microdomains in thin BCP films during SVA.

SVA has emerged recently as an effective and versatile tool to control and manipulate the self-assembly of BCPs in thin

*Current Address: Ilja Gunkel, Adolphe Merkle Institute, Chemin Des Verdiers 4, CH-1700 Fribourg, Switzerland

†Current Address: Xiaodan Gu, Department of Chemical Engineering, Stanford University, 443 via Ortega, Stanford, California 94305

‡Ilja Gunkel and Xiaodan Gu contributed equally to this work

In memoriam: This article was written in honor of E. J. Kramer. He was a good friend, great collaborator and an admirable competitor.

Additional Supporting Information may be found in the online version of this article.

© 2015 Wiley Periodicals, Inc.

films.³ The mobility of polymer chains is strongly enhanced in the presence of solvent vapor, which facilitates the lateral ordering of the BCP microdomains in films on planar substrates.^{4–7} Furthermore, microdomains with high degrees of alignment can be generated by means of SVA of BCP thin films on topographically patterned substrates,^{8–13} or by applying soft shear during SVA.^{14,15} In order for BCPs to self-assemble in thin films by means of SVA, polymer chains have to be sufficiently mobile, which is realized for solvent concentrations at which the glass transition temperatures of the blocks are below room temperature.^{16–18} In the case of nonselective or partially selective solvents, increasing the solvent concentration not only increases the chain mobility but also leads to an increased screening of the nonfavorable interactions between segments of different blocks by the solvent. At sufficiently high solvent concentrations, screening of the interactions can induce a disordering of the BCP.¹⁹ Within a window of solvent concentrations between vitrification and disordering of the film, the microdomain spacing can be precisely tuned by adjusting the solvent concentration in the BCP thin film. Smaller domain spacings are observed at higher solvent concentrations resulting from relaxation of the copolymer chain at the interface between different blocks due to the increase in screening of the nonfavorable interactions between segments of different blocks by the solvent.^{12,13,18,20} Furthermore, increasing the solvent concentration has been shown to reduce the number of defects and increase the grain size in thin films of BCPs with cylindrical microdomains oriented parallel to¹⁸ or normal to the substrate surface.⁷ The largest grain sizes were obtained in films that were annealed at solvent concentrations close to the order–disorder transition (ODT). Recent simulations of SVA in lamellar BCPs show that the defect density can be further reduced by first driving the film into the disordered state in order to efficiently remove processing-related defects before annealing the BCP at solvent concentrations below (but close to) the ODT.²¹

SVA enables tuning the morphology of BCPs in thin films by adjusting the solvent selectivity. The addition of a selective solvent changes the effective volume fractions of the components, which can lead to order–order transitions and to a stabilization of morphologies that do not correspond to the volume fraction of the components in the original BCP.²² Transitions from cylinders to spheres,^{8,17,23} from cylinders to perforated lamellae,¹² and from gyroid to cylinders²⁴ have been reported for BCP films upon annealing in selective solvent vapors. A wide range of morphologies can be obtained from the same BCP by means of SVA with either solvents of different selectivity,¹³ mixtures of selective solvents,^{25,26} or with mixed vapors of solvents with different selectivity for the respective blocks.²⁷

Detailed structural information of BCP films in the swollen state, or as solvent is removed can be obtained by means of *in situ* grazing-incidence small-angle X-ray scattering (GISAXS).^{28,29} *In situ* GISAXS measurements were shown to allow for investigations of the reorganization,^{16,30,31} reorientation,^{32–34} and lateral ordering^{19,35} of BCP microdomains during swelling and solvent removal. Furthermore, *in situ*

GISAXS was used to monitor real-time morphological transitions in BCP films during SVA.^{17,26}

Here, we used *in situ* GISAXS to study the packing of spherical microdomains in thin films of poly(styrene-*b*-4-vinylpyridine) (PS-*b*-P4VP) BCPs during annealing in PS-selective tetrahydrofuran (THF) vapor. We show that swollen 180 nm thick films (8–9 layers) undergo a transition from hexagonal to orthorhombic packing upon deswelling. The orthorhombic phase was found to be stable only at ~ 7 layers. Dried films exhibited structures with coexisting hexagonal and orthorhombic symmetries.

EXPERIMENTAL

PS-*b*-P4VP BCPs with a total molecular weight of $M_n = 19\text{-}b\text{-}5.2 \text{ kg mol}^{-1}$ were purchased from Polymer Source and used as received. Bulk PS-*b*-P4VP samples show a cylindrical morphology upon thermal annealing as confirmed by small-angle X-ray scattering measurements (Supporting Information, Fig. S1). PS-*b*-P4VP was dissolved in a toluene/THF (Sigma-Aldrich) solvent mixture at a volume ratio of 70:30 to avoid micelle formation.³⁶ PS-*b*-P4VP thin films with a thickness of $69 \pm 1 \text{ nm}$ were prepared by spin coating 1.4% w/v solutions of PS-*b*-P4VP in toluene/THF (70:30) at 1750 rpm for 20 s onto silicon wafers with a native oxide layer. The wafers were cut into pieces $\sim 20 \times 20 \text{ mm}^2$ in size for *in situ* GISAXS measurements during SVA.

PS-*b*-P4VP thin films were annealed in THF vapor using a custom-designed chamber that was described previously.¹⁸ THF was injected into the annealing chamber, and the degree of swelling of a film was controlled by adjusting the flow rate of dry nitrogen into the annealing chamber using a Cole Parmer flow meter (flow rate (N₂) 150 sccm). Deswelling of a swollen film was achieved by increasing the nitrogen flow rate. Removing the chamber cover resulted in instantaneous evaporation of solvent in the chamber, which, in turn, caused rapid drying of the films. The polymer volume fraction ϕ_{BCP} in the swollen film was determined based on real-time film thickness measurements using a Filmetrics F20 spectroscopic white light reflectometer and was calculated as follows:

$$\phi_{\text{BCP}} = \frac{t_0}{t} = \frac{1}{X_{\text{SR}}}, \quad (1)$$

where t_0 is the thickness of the dry (as spun) film, t is the thickness of the swollen film and X_{SR} denotes the swelling ratio.

GISAXS experiments were conducted at Beamline 7.3.3 at the Advanced Light Source (ALS) of Lawrence Berkeley National Laboratory (LBNL) at an X-ray energy of 10 keV.³⁷ The sample-to-detector distance was calibrated with a silver behenate standard. GISAXS measurements were taken at a fixed incidence angle of 0.14° and scattering images were collected on a Pilatus 1M 2D pixel detector (Dectris). For *in situ* GISAXS experiments during annealing of PS-*b*-P4VP thin films in THF vapor the annealing chamber was mounted on a Huber 5203.10 2-circle goniometric stage and measurements were performed at a

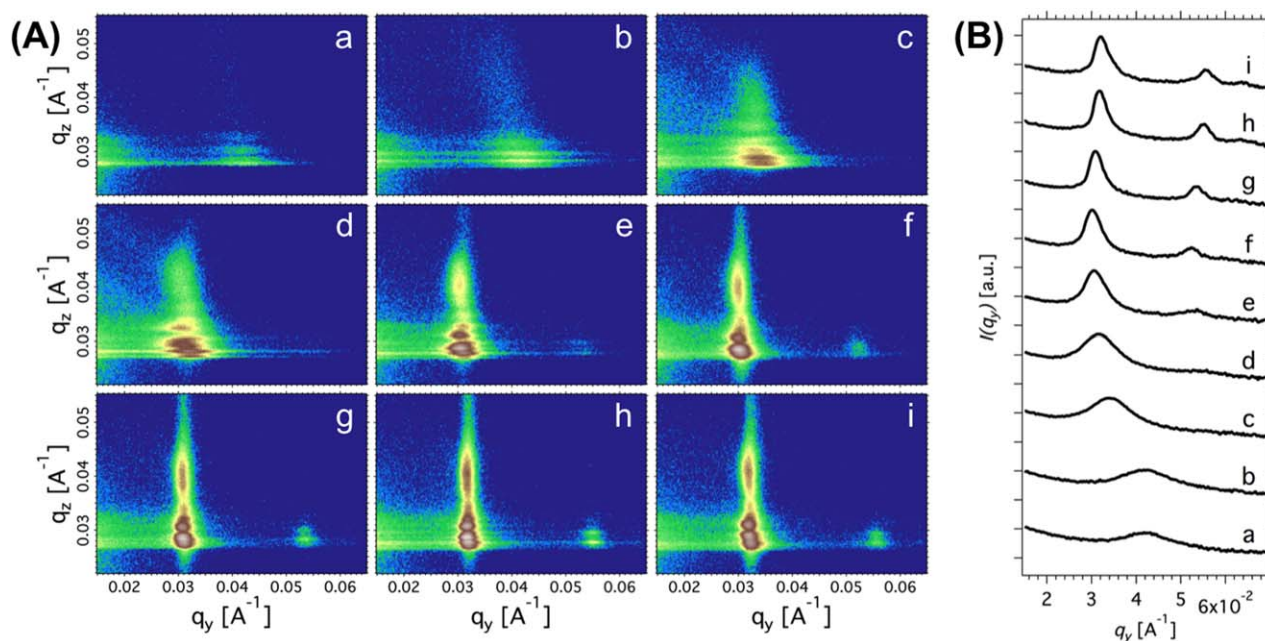


FIGURE 1 (A) 2D *in situ* GISAXS data obtained during swelling of PS-*b*-P4VP films in THF vapor. (B) Corresponding in-plane profiles. The different 2D images and respective line profiles correspond to different polymer volume fractions ϕ_{BCP} in the swollen films. a: $\phi_{\text{BCP}} = 1.0$ ($t_0 = 69$ nm); b: $\phi_{\text{BCP}} = 0.750$; c: $\phi_{\text{BCP}} = 0.657$; d: $\phi_{\text{BCP}} = 0.580$; e: $\phi_{\text{BCP}} = 0.519$; f: $\phi_{\text{BCP}} = 0.463$; g: $\phi_{\text{BCP}} = 0.426$; h: $\phi_{\text{BCP}} = 0.394$; i: $\phi_{\text{BCP}} = 0.379$. The in-plane profiles were shifted vertically for clarity.

temperature of 22.7 ± 0.3 °C. Individual exposure times were 20 s and the delay between successive exposures was 40 s. The sample was being moved to a previously unexposed area after three exposures to avoid beam damage of the sample.

The 2D GISAXS images were calibrated and reduced using Nika for IGOR Pro (Wavemetrics).³⁸ A profile of intensity $I(q_y)$ was extracted from the 2D scattering data by line integration at $q_z = 0.0287 \pm 0.0042$ Å⁻¹, where q_z is the out-of-plane scattering vector and q_y is the in-plane scattering vector. The in-plane profiles were fit with the following function

$$I(q_y) = I_0 + cq_y^{-d} + \sum_{i=1}^n h_i \frac{1}{1 + ((q_y - q_{y,i})/b_i)^2} \quad (2)$$

where the background is subtracted using a power law. The sum of Lorentzian functions in eq 2 served to obtain the peak positions $q_{y,i}$, peak widths b_i , and peak amplitudes h_i of n maxima in the in-plane profiles. The calculation of the in-plane domain spacing d and *FWHM* of the first order in-plane reflection is straightforward:

$$d = \frac{2\pi}{q_{y,1}} \quad (3)$$

$$\text{FWHM} = 2b_1. \quad (4)$$

RESULTS AND DISCUSSION

Swelling: *In Situ* GISAXS

Figure 1A shows a series of 2D *in situ* GISAXS images that were collected during swelling of thin PS-*b*-P4VP films in

THF vapor at a swelling rate of 1.90 nm min⁻¹. The corresponding in-plane profiles are shown in Figure 1B. The as-spun film ($\phi_{\text{BCP}} = 1.0$, $t_0 = 69$ nm) showed a relatively broad first-order in-plane reflection indicating the lateral order of microdomains was only short-range. Fast solvent evaporation during spin coating leads to the formation of microdomains that lack long-range order due to kinetically limited chain motion.³⁹ PS-*b*-P4VP films did not show any significant reorganization upon swelling up to concentrations of $\phi_{\text{BCP}} = 0.75$ as can be seen from the almost unchanged position of the first-order peak. At this concentration the glass transition temperature of P4VP is about 12 °C and that of PS is -9 °C, which was estimated using the Fox equation (Supporting Information Fig. S2). Note that the actual polymer concentration in the P4VP domains is likely to be higher than the measured ϕ_{BCP} value due to selectivity of THF for PS. At $\phi_{\text{BCP}} = 0.657$ the position of the first-order reflection shifted to significantly lower q_y values indicating that chain mobility is sufficiently high for structural rearrangement. In addition, the peak intensity increased and the width of the peak decreased due to an increased microdomain correlation length. The increased film thickness of the swollen film ($t = 105$ nm) resulted in an increased number of fringes in the out-of-plane direction (see c in Fig. 1A). With further swelling of the film ($\phi_{\text{BCP}} = 0.580$), the intensity of the first-order peak further increased and the peak position continued to shift to lower q_y values. At $\phi_{\text{BCP}} = 0.519$ the width of the first-order reflection became narrower and a second-order peak was observed indicating well-ordered microdomains in the thin film. As will be discussed in more detail below, the 2nd-to-1st-order peak ratio corresponds to

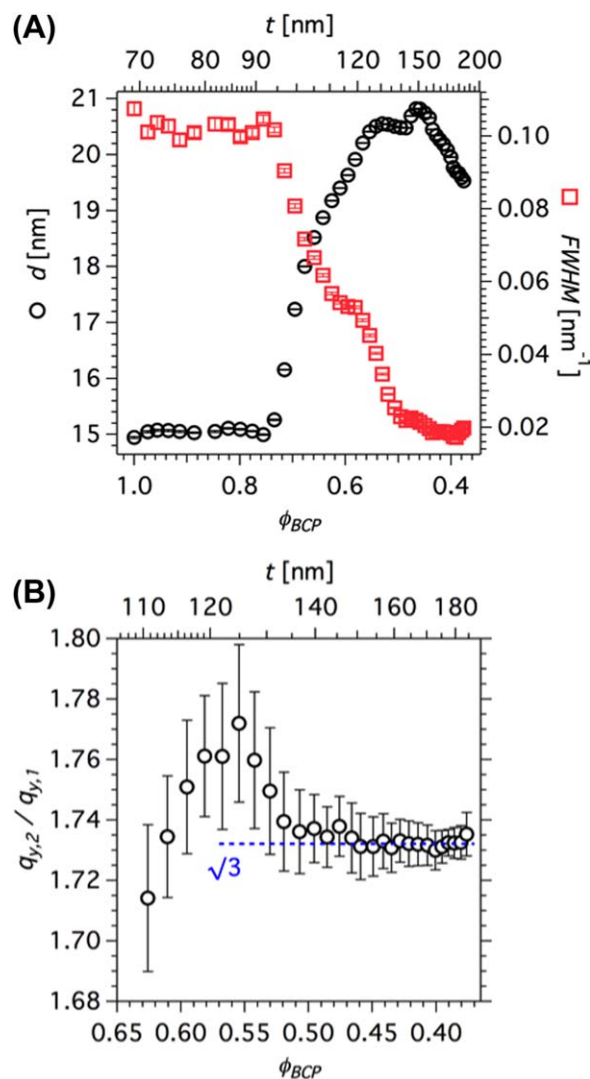


FIGURE 2 Characterization of the in-plane structure in PS-*b*-P4VP films during swelling in THF vapor. (A) Domain spacing d (open spheres with error bars) and $FWHM$ (open squares with error bars) in the in-plane scattering profiles $I(q_y)$ as a function of the polymer volume fraction ϕ_{BCP} (swollen film thickness). (B) Ratio of second-to-first order peak positions $q_{y,2}/q_{y,1}$ (open spheres with error bars) in the $I(q_y)$ profiles as a function of ϕ_{BCP} .

hexagonally packed microdomains. As the swelling increased from $\phi_{BCP} = 0.519$ to $\phi_{BCP} = 0.379$ the hexagonal in-plane symmetry was maintained, while the position of the first-order peak slightly shifted to larger q_y values, corresponding to a smaller in-plane spacing.

In order to further characterize the in-plane structure during swelling, the $I(q_y)$ profiles shown in Figure 1B were fit to eq 2. The in-plane domain spacing d and $FWHM$ of the first-order peak were calculated by eqs 3 and 4 using the $q_{y,i}$ and b_1 values from the fits. Figure 2A shows the domain spacing d and $FWHM$ as a function of the polymer volume fraction ϕ_{BCP} . Figure 2B shows the 2nd-to-1st-order peak ratio $q_{y,2}/q_{y,1}$ as a

function of ϕ_{BCP} . The domain spacing and $FWHM$ remained unchanged for $\phi_{BCP} > 0.75$, indicating insufficient chain mobility for any rearrangement of microdomains in the plane of the film (Fig. 2A). The domain spacing increased from 15.0 to 20.5 nm when the film was swollen from $\phi_{BCP} = 0.75$ to 0.55. The increase in domain spacing is accompanied by a drop in the $FWHM$ resulting from an increase of the microdomain correlation length. The increased correlation length is consistent with the occurrence of a second-order peak for $\phi_{BCP} < 0.63$ (Fig. 2B). After structural equilibration ($0.63 > \phi_{BCP} > 0.50$) the microdomain packing approached hexagonal symmetry at $\phi_{BCP} \sim 0.50$ that is given by $q_{y,2}/q_{y,1} = \sqrt{3}$. The domain spacing d continued to increase for $0.63 > \phi_{BCP} > 0.55$, then remained constant for $0.55 > \phi_{BCP} > 0.49$, and decreased for $0.47 > \phi_{BCP} > 0.38$. The $FWHM$ further decreased for $0.55 > \phi_{BCP} > 0.49$ and then remained almost unchanged for $0.47 > \phi_{BCP} > 0.38$. The film was found to form an array of hexagonally packed microdomains in a film thickness range from $t = 140$ to 182 nm ($q_{y,2}/q_{y,1} = \sqrt{3}$ for $0.49 > \phi_{BCP} > 0.38$ in Fig. 2B). In this range the domain spacing decreased from $d = 20.8$ to 19.5 nm. This corresponds to 7–9 layers based on a simple calculation of t/d (assuming spherical microdomains oriented parallel to the substrate).

Deswelling: *In Situ* GISAXS

Figure 3A shows a series of 2D *in situ* GISAXS images that were collected during deswelling a swollen, 182 nm thick ($\phi_{BCP} = 0.379$) PS-*b*-P4VP film in THF vapor at a deswelling (solvent removal) rate of $-2.80 \text{ nm min}^{-1}$. The corresponding in-plane profiles are shown in Figure 3B. In the beginning of the deswelling process the film showed hexagonal symmetry as confirmed by $q_{y,2}/q_{y,1} = \sqrt{3}$ (see Figs. 3B and 4B). Deswelling to $\phi_{BCP} = 0.416$ resulted in the formation of additional in-plane reflections between the two peaks observed for hexagonally packed microdomains. The 2D GISAXS image appears similar to the results obtained by Kramer and coworkers for the orthorhombic packing of spheres in thin films of thermally annealed PS-*b*-P2VP BCPs.¹ Here, the orthorhombic symmetry was induced by deswelling a film with an array of hexagonally packed spheres.

Further deswelling of the film ($\phi_{BCP} = 0.466$) resulted in a more pronounced separation of the 1st- and 2nd-order reflections (Fig. 3A and B). At even smaller film thickness ($t < 141$ nm, $\phi_{BCP} > 0.489$) the 1st- and 2nd-order peaks started to merge again and ultimately overlapped in the dry film. This, in combination with the decreased intensity of higher order peaks and the increased $FWHM$, indicates that orthorhombic in-plane packing of (spherical) microdomains is not stable in thinner films ($t < 141$ nm, $\phi_{BCP} > 0.489$).

To further characterize the symmetry transition from hexagonal to orthorhombic in-plane microdomain packing during deswelling, the $I(q_y)$ profiles shown in Figure 3 were fit to eq 2. The in-plane domain spacing d and $FWHM$ of the first-order peak were calculated by eqs 3 and 4 using the $q_{y,i}$ and b_1 values from the fits. Figure 4 shows the domain spacing d , $FWHM$, and peak ratio of the (10) and (01) reflections,

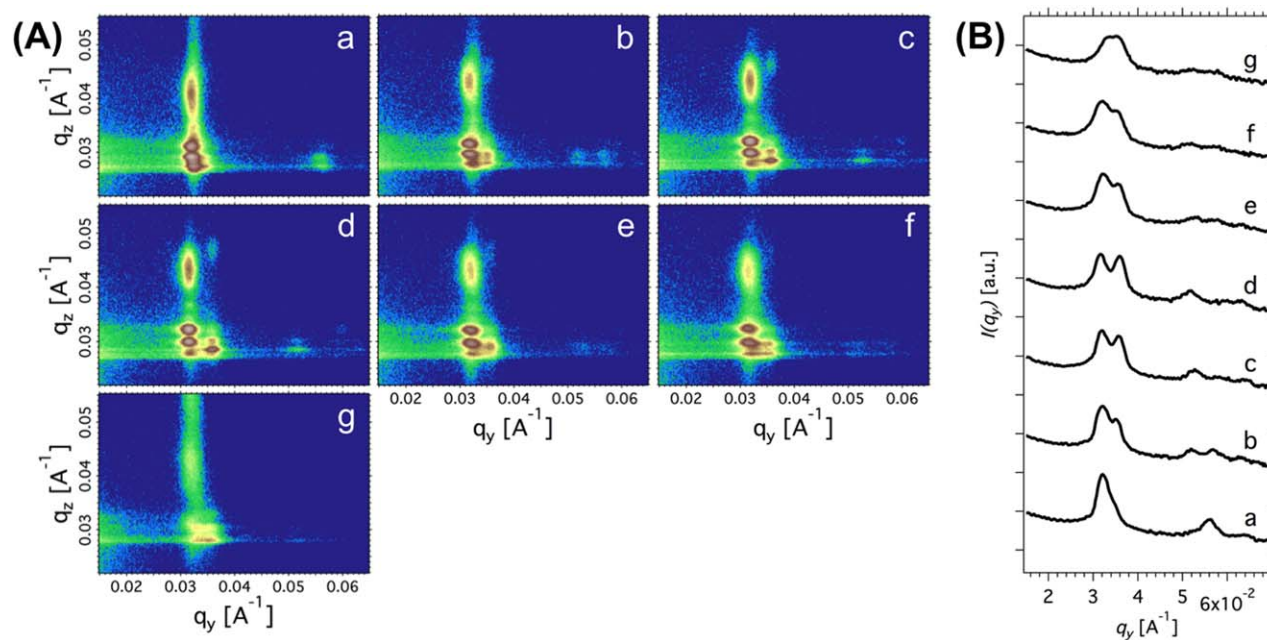


FIGURE 3 (A) 2D *in situ* GISAXS data obtained during deswelling of PS-*b*-P4VP films in THF vapor. (B) Corresponding $I(q_y)$ profiles. The different 2D images and respective line profiles correspond to different polymer volume fractions ϕ_{BCP} in the swollen films. a: $\phi_{\text{BCP}} = 0.383$; b: $\phi_{\text{BCP}} = 0.416$; c: $\phi_{\text{BCP}} = 0.460$; d: $\phi_{\text{BCP}} = 0.466$; e: $\phi_{\text{BCP}} = 0.489$; f: $\phi_{\text{BCP}} = 0.535$; g: $\phi_{\text{BCP}} = 1.00$. The in-plane profiles were shifted vertically for clarity.

q_{10}/q_{01} , as a function of the polymer volume fraction ϕ_{BCP} . Interestingly, during deswelling the domain spacing d remained almost unchanged with a small peak at $t = 148$ nm. This is in contrast to the behavior observed during deswelling in neutral solvents, where only the polymer concentration determines values of the domain spacing, which are identical for swelling and deswelling.^{18,20} It is not clear whether the difference in domain spacings between swelling and deswelling shown in Figure 4A is related to the formation of the (metastable) orthorhombic packing of spheres in the film or the different evaporation rates of PS-selective THF from the PS and P4VP domains. The *FWHM* values were found to be similar during swelling and deswelling indicating similar microdomain correlation lengths for orthorhombic (deswelling) and hexagonal (swelling) packing of spheres.

The in-plane symmetry can be further characterized by the lattice vectors or the peak ratio of the (10) and (01) reflections, q_{10}/q_{01} . In a hexagonal structure the two lattice vectors are equal, and thus $q_{10}/q_{01} = 1$, while in the case of the in-plane symmetry corresponding to the bcc(110) plane, $q_{10}/q_{01} = (4/3)^{1/2} \sim 1.155$. Thermally annealed spherical PS-*b*-P2VP BCPs are hexagonal in films 1–3 layers thick, while films thicker than 23 layers are bcc. The in-plane packing of spheres in films of 4–23 layers is face-centered orthorhombic (fco) and asymptotically approaches the symmetry of the bcc(110) in-plane as the number of layers is increased ($q_{10}/q_{01} \sim 1.08$ for 4 layers and $q_{10}/q_{01} \sim 1.15$ for 12 layers). At 4 layers hexagonal and fco structures were found to coexist.

¹ It was shown that the transition from hexagonal (hex) to fco packing is suppressed in blends of PS-*b*-P2VP and PS homopolymer extending the hex-to-fco transition beyond 4 layers with the critical layer thickness increasing with increasing homopolymer weight fraction. Figure 4B shows the peak ratio of the (10) and (01) reflections, q_{10}/q_{01} , as a function of the polymer volume fraction ϕ_{BCP} in PS-*b*-P4VP films during swelling and deswelling in PS-selective THF vapor. During swelling and for $\phi_{\text{BCP}} < 0.65$ the structure in the films was hexagonal as indicated by $q_{10}/q_{01} = 1$, whereas deswelling induced a transition from hexagonal to fco packing at $\phi_{\text{BCP}} \sim 0.40$ as can be seen from a discontinuous jump of q_{10}/q_{01} to ~ 1.08 . The peak ratio continued to increase as the film deswelled further and reached a maximum of $q_{10}/q_{01} \sim 1.13$ at $\phi_{\text{BCP}} \sim 0.47$. At higher polymer concentrations, $\phi_{\text{BCP}} > 0.47$, the peak ratio decreased to $q_{10}/q_{01} \sim 1.10$.

Deswelling PS-*b*-P4VP in PS-selective THF induced a transition from hexagonal to face-centered orthorhombic symmetry in 170 nm thick films corresponding to ~ 9 layers. The fco structure deforms to approach bcc(110) in-plane symmetry upon deswelling the film to a thickness of 148 nm, which corresponds to ~ 7.5 layers. The fco packing of spheres is sensitive to the polymer concentration and the film thickness. Both are continuously changing during deswelling rendering the fco structure unstable during solvent removal. This results in coexisting hexagonal and fco structures in dry films after slow deswelling.

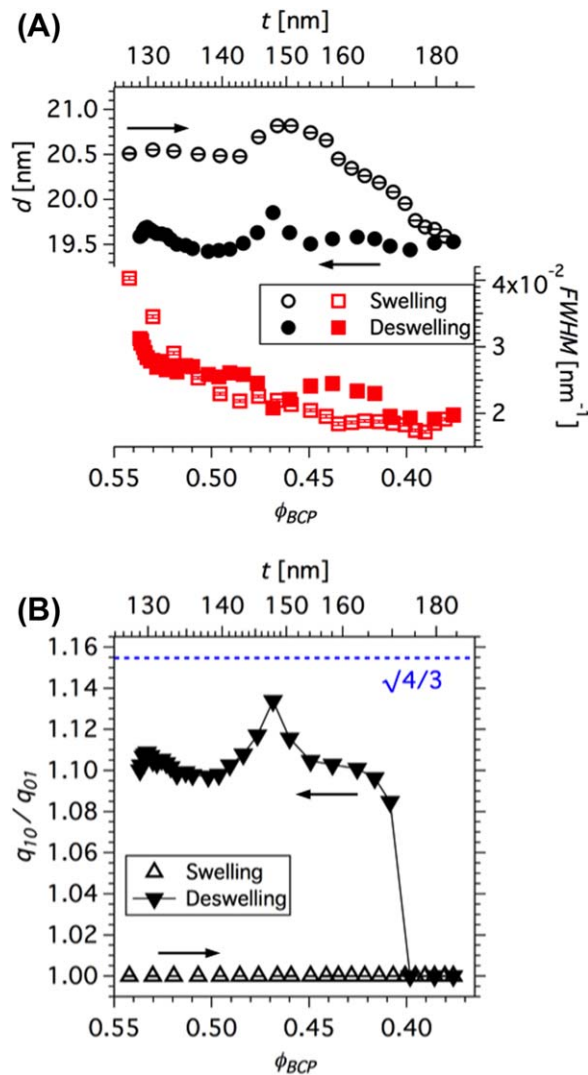


FIGURE 4 Characterization of the in-plane structure in PS-*b*-P4VP films during deswelling (open symbols with error bars) in THF vapor. The corresponding swelling data (filled symbols) are shown for direct comparison. (A) Domain spacing d and $FWHM$ in the in-plane scattering profiles $I(q_v)$ as a function of the polymer volume fraction ϕ_{BCP} (swollen film thickness). (B) Peak ratio of the (10) and (01) reflections, q_{10}/q_{01} , as a function of ϕ_{BCP} .

To study the effect of the deswelling rate on the sphere packing, films were deswelled at different rates as shown in Figure 5. All films were first swollen to around 183 nm followed by deswelling at different deswelling rates. Interestingly, the domain spacing was found to depend strongly on the solvent removal rate. While in films that were deswelled slowly (2.5 nm min^{-1}) the domain spacing remained almost unchanged around $19.6 \pm 0.2 \text{ nm}$, d significantly decreased from 19.5 to 17.7 nm upon deswelling at a higher rate of 16.8 nm min^{-1} (Fig. 5A). The domain spacing was decreased even more (from 19.5 to 16 nm) when the solvent was removed instantaneously. Note that for neutral solvents solvent removal leads to increased domain spacing values.

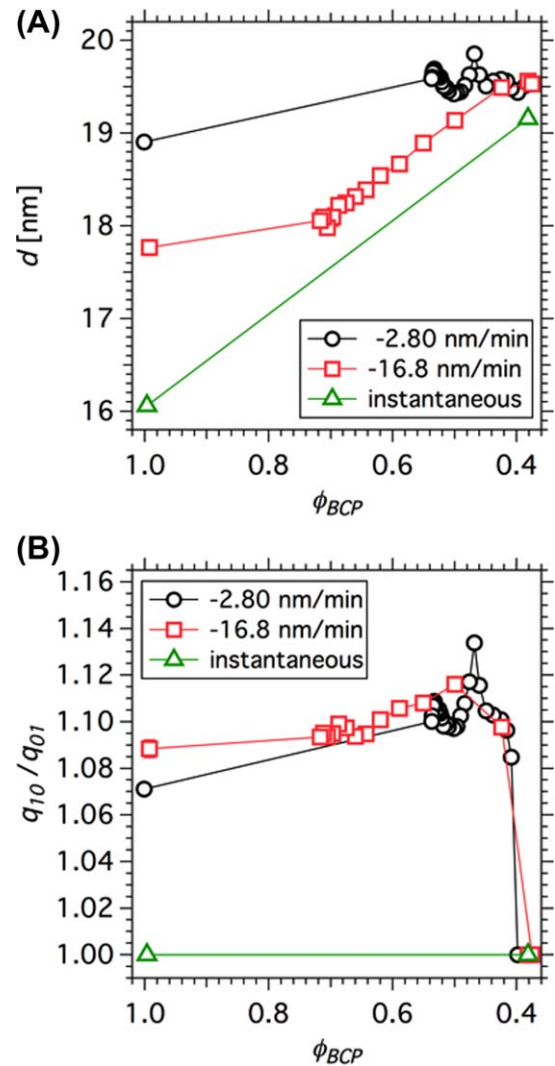


FIGURE 5 Characterization of the in-plane structure in PS-*b*-P4VP films during deswelling (open symbols) in THF vapor at different deswelling rates. (A) Domain spacing d in the in-plane scattering profiles $I(q_v)$ as a function of the polymer volume fraction ϕ_{BCP} (swollen film thickness). (B) Peak ratio of the (10) and (01) reflections, q_{10}/q_{01} , as a function of ϕ_{BCP} .

Here, removal of the PS-selective THF resulted in significantly smaller values of the domain spacing. We speculate that changes of the relative volume fraction resulting from different solvent removal rates of THF in PS and P4VP domains induce the observed changes in the domain spacing.

Figure 5B shows the peak ratio of the (10) and (01) reflections, q_{10}/q_{01} , as a function of the polymer volume fraction ϕ_{BCP} in PS-*b*-P4VP films during deswelling at different deswelling rates. The maximum in q_{10}/q_{01} was found to decrease with increasing deswelling rate. Furthermore, the hex-to-fcc transition was suppressed in case of instantaneous solvent removal resulting in the formation of a hexagonal structure in the dry film (Fig. 6), whereas slow deswelling resulted in coexisting hexagonal and fcc symmetries.

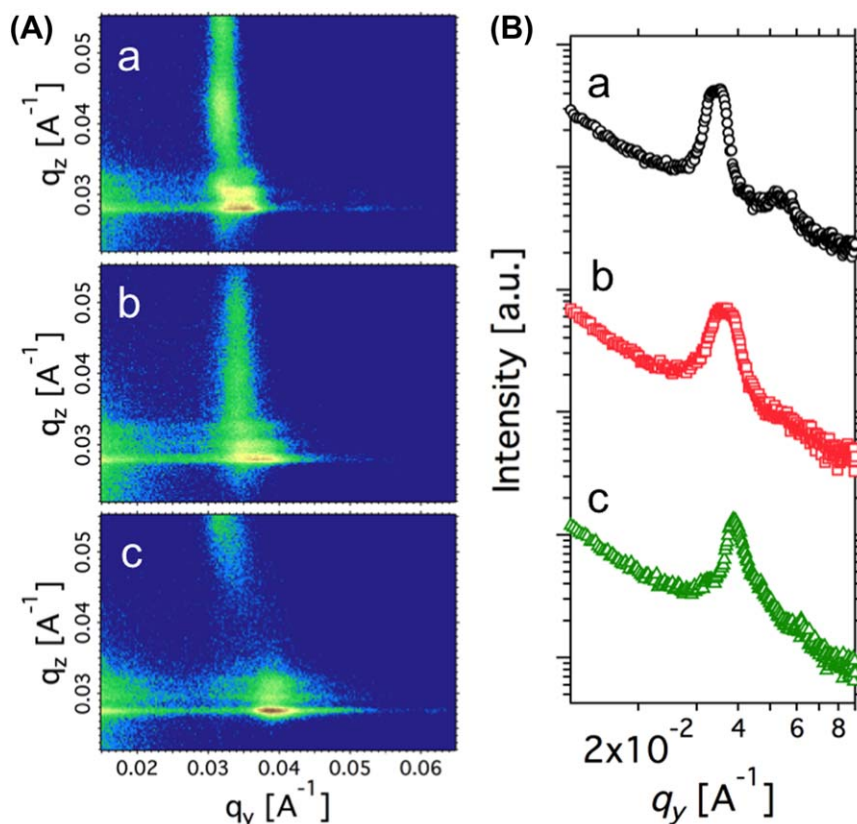


FIGURE 6 GISAXS data [(A): 2D images and (B): in-plane profiles] of dry PS-*b*-P4VP films. The different 2D images and corresponding line profiles correspond to different deswelling rates of swollen films. a: $-2.80 \text{ nm min}^{-1}$; b: $-16.8 \text{ nm min}^{-1}$; c: instantaneous solvent removal; The in-plane profiles were shifted vertically for clarity.

Generally, in case of selective SVA solvent removal induced structures with short-range order as can be seen from the large peak widths in $I(q_y)$ profiles in dry films (Fig. 6B). Deswelling-induced structural transitions and deterioration of in-plane order of spherical microdomains are strongly related to changes in the polymer volume fraction and concentration-dependent stability of in-plane packing of spheres.

CONCLUSIONS

We studied swelling and deswelling of asymmetric PS-*b*-P4VP BCPs by means of *in situ* GISAXS. PS-*b*-P4VP was found to form hexagonally packed spheres upon swelling in PS-selective THF vapor. Deswelling films at slow rates induced a transition from hexagonal to face-centered orthorhombic packing of spheres. Our results show the importance of *in situ* GISAXS for tracking structural transitions in BCP films during selective SVA. Furthermore, *in situ* GISAXS measurements reveal a dilemma: structures induced by selective swelling are very hard to be maintained in films after solvent removal. Selective swelling and deswelling can induce symmetry changes, changes of domain spacing, and strong deterioration of the in-plane order as well as out-of-plane packing of microdomains.

ACKNOWLEDGMENTS

This work was supported by the U.S. Department of Energy BES under contract DE-FG02-96ER45612. Beamline 7.3.3 of the Advanced Light Source is supported by the Director of the Office of Science, Office of Basic Energy Sciences, of the U.S. Department of Energy under Contract No. DE-AC02-05CH11231. I. Gunkel acknowledges the support by the ALS Postdoctoral Fellowship program. X. Gu acknowledges an ALS Doctoral Fellowship program for providing partial financial support. A. Hexemer was supported by a DOE Early Career Research Program grant. The authors also gratefully acknowledge the assistance of E. Lim, P. Stewart, Jr., and C. Zhu with GISAXS measurements.

REFERENCES AND NOTES

- 1 G. E. Stein, E. J. Kramer, X. Li, J. Wang, *Macromolecules* **2007**, *40*, 2453–2460.
- 2 G. E. Stein, E. W. Cochran, K. Katsov, G. H. Fredrickson, E. J. Kramer, X. Li, J. Wang, *Phys. Rev. Lett.* **2007**, *98*, 158302
- 3 C. Sinturel, M. Vayer, M. Morris, M. A. Hillmyer, *Macromolecules* **2013**, *46*, 5399–5415.
- 4 S. H. Kim, M. J. Misner, T. Xu, M. Kimura, T. P. Russell, *Adv. Mater.* **2004**, *16*, 226–231.
- 5 S. Park, J. Y. Wang, B. Kim, J. Xu, T. P. Russell, *ACS Nano* **2008**, *2*, 766–772.

- 6 S. Park, B. Kim, J. Xu, T. Hofmann, B. M. Ocko, T. P. Russell, *Macromolecules* **2009**, *42*, 1278–1284.
- 7 A. Baruth, M. Seo, C. H. Lin, K. Walster, A. Shankar, M. A. Hillmyer, C. Leighton, *ACS Appl. Mater. Interfaces* **2014**, *6*, 13770–13781.
- 8 J. K. Bosworth, M. Y. Paik, R. Ruiz, E. L. Schwartz, J. Q. Huang, A. W. Ko, D. M. Smilgies, C. T. Black, C. K. Ober, *ACS Nano* **2008**, *2*, 1396–1402.
- 9 S. Park, D. H. Lee, J. Xu, B. Kim, S. W. Hong, U. Jeong, T. Xu, T. P. Russell, *Science* **2009**, *323*, 1030–1033.
- 10 S. W. Hong, J. Huh, X. Gu, D. H. Lee, W. H. Jo, S. Park, T. Xu, T. P. Russell, *Proc. Natl. Acad. Sci. USA* **2012**, *109*, 1402–1406.
- 11 C. Cummins, R. A. Kelly, A. Gangnaik, Y. M. Georgiev, N. Petkov, J. D. Holmes, M. A. Morris, *Macromol. Rapid Commun.* **2015**, *36*, 762–767.
- 12 Y. S. Jung, C. A. Ross, *Adv. Mater.* **2009**, *21*, 2540–2545.
- 13 J. W. Jeong, W. I. Park, M. J. Kim, C. A. Ross, Y. S. Jung, *Nano Lett.* **2011**, *11*, 4095–4101.
- 14 Z. Qiang, L. Zhang, G. E. Stein, K. A. Cavicchi, B. D. Vogt, *Macromolecules* **2014**, *47*, 1109–1116.
- 15 Z. Qiang, Y. Zhang, J. A. Groff, K. A. Cavicchi, B. D. Vogt, *Soft Matter* **2014**, *10*, 6068–6076.
- 16 Z. Di, D. Posselt, D. M. Smilgies, C. M. Papadakis, *Macromolecules* **2010**, *43*, 418–427.
- 17 M. Y. Paik, J. K. Bosworth, D. M. Smilgies, E. L. Schwartz, X. Andre, C. K. Ober, *Macromolecules* **2010**, *43*, 4253–4260.
- 18 X. Gu, I. Gunkel, A. Hexemer, W. Gu, T. P. Russell, *Adv. Mater. Weinheim.* **2014**, *26*, 273–281.
- 19 S. H. Kim, M. J. Misner, L. Yang, O. Gang, B. M. Ocko, T. P. Russell, *Macromolecules* **2006**, *39*, 8473–8479.
- 20 X. Gu, I. Gunkel, A. Hexemer, T. P. Russell, *Colloid Polym. Sci.* **2014**, *292*, 1795–1802.
- 21 S. M. Hur, G. S. Khaira, A. Ramírez-Hernández, M. Müller, P. F. Nealey, J. J. de Pablo, *ACS Macro Lett.* **2015**, *4*, 11–15.
- 22 C. Lai, W. B. Russel, R. A. Register, *Macromolecules* **2002**, *35*, 841–849.
- 23 Y. Wang, X. Hong, B. Liu, C. Ma, C. Zhang, *Macromolecules* **2008**, *41*, 5799–5808.
- 24 M. S. She, T. Y. Lo, R. M. Ho, *Macromolecules* **2014**, *47*, 175–182.
- 25 W. Bai, A. F. Hannon, K. W. Gotrik, H. K. Choi, K. Aissou, G. Lontos, K. Ntetsikas, A. Alexander-Katz, A. Avgeropoulos, C. A. Ross, *Macromolecules* **2014**, *47*, 6000–6008.
- 26 M. A. Chavis, D. M. Smilgies, U. B. Wiesner, C. K. Ober, *Adv. Funct. Mater.* **2015**, *25*, 3057–3065.
- 27 K. W. Gotrik, A. F. Hannon, J. G. Son, B. Keller, A. Alexander-Katz, C. A. Ross, *ACS Nano.* **2012**, *6*, 8052–8059.
- 28 D. M. Smilgies, P. Busch, C. M. Papadakis, D. Posselt, *Synchrotron Radiation News*, **2002**, *15*, 35–42.
- 29 A. Hexemer, P. Müller-Buschbaum, *IUCrJ* **2015**, *2*, 106–125.
- 30 C. M. Papadakis, Z. Di, D. Posselt, D. M. Smilgies, *Langmuir* **2008**, *24*, 13815–13818.
- 31 Z. Di, D. Posselt, D. M. Smilgies, R. Li, M. Rauscher, I. I. Potemkin, C. M. Papadakis, *Macromolecules* **2012**, *45*, 5185–5195.
- 32 K. A. Cavicchi, K. J. Berthiaume, T. P. Russell, *Polymer* **2005**, *46*, 11635–11639.
- 33 K. A. Cavicchi, T. P. Russell, *Macromolecules* **2007**, *40*, 1181–1186.
- 34 E. B. Gowd, M. Böhme, M. Stamm, *IOP Conf. Ser.: Mater. Sci. Eng.* **2010**, *14*, 012015
- 35 S. H. Kim, M. J. Misner, T. P. Russell, *Adv. Mater.* **2008**, *20*, 4851–4856.
- 36 S. Park, J. Y. Wang, B. Kim, W. Chen, T. P. Russell, *Macromolecules* **2007**, *40*, 9059–9063.
- 37 A. Hexemer, W. Bras, J. Glossinger, E. Schaible, E. Gann, R. Kirian, A. MacDowell, M. Church, B. Rude, H. Padmore, *J. Phys.: Conf. Ser.* **2010**, *247*, 012007
- 38 J. Ilavsky, *J. Appl. Crystallogr.* **2012**, *45*, 324–328.
- 39 G. Kim, M. Libera, *Macromolecules* **1998**, *31*, 2569–2577.